A high-resolution infrared spectroscopic investigation of the halogen atom-HCN entrance channel complexes solvated in superfluid helium droplets

Jeremy M. Merritt,* Jochen Küpper,§ and Roger E. Miller†
Department of Chemistry, University of North Carolina at Chapel Hill, Chapel Hill, NC 27599
(Dated: October 9, 2006)

Rotationally resolved infrared spectra are reported for the X-HCN (X = Cl, Br, I) binary complexes solvated in helium nanodroplets. These results are directly compared with that obtained previously for the corresponding X-HF complexes [J. M. Merritt, J. Küpper, and R. E. Miller, PCCP, 7, 67 (2005)]. For bromine and iodine atoms complexed with HCN, two linear structures are observed and assigned to the $^2\Sigma_{1/2}$ and $^2\Pi_{3/2}$ ground electronic states of the nitrogen and hydrogen bound geometries, respectively. Experiments for HCN + chlorine atoms give rise to only a single band which is attributed to the nitrogen bound isomer. That the hydrogen bound isomer is not stabilized is rationalized in terms of a lowering of the isomerization barrier by spin-orbit coupling. Theoretical calculations with and without spin-orbit coupling have also been performed and are compared with our experimental results. The possibility of stabilizing high-energy structures containing multiple radicals is discussed, motivated by preliminary spectroscopic evidence for the di-radical Br-HCCCN-Br complex. Spectra for the corresponding molecular halogen HCN-X_2 complexes are also presented.

INTRODUCTION

Much of our knowledge of intermolecular forces has come from the high-resolution spectroscopy of weakly bound closed shell complexes [1], and there is considerable promise that similar advances can be made for open shell complexes. Experimentally, the study of open shell reactive molecular complexes is more difficult than their closed shell counterparts due to the fact that their tendency to react must also be surpressed. The cooling provided by free jet expansion [2, 3, 4] and matrix isolation [5, 6, 7] is sometimes sufficient to stabilize complexes of this type. Recently, nano-scale liquid helium droplets have also emerged as a nearly ideal spectroscopic matrix for the study of highly metastable species [8, 9, 10, 11], including the stabilization of pre- and post-reactive cluster systems [12, 13, 14]. Such weakly bound complexes sample the long range van der Waals forces in the entrance and exit channel regions of the potential energy surface, which have recently been shown to strongly influence the reaction dynamics of Cl + HD [15, 16, 17] and the near threshold photo-dissociation of formaldehyde [18, 19]. Despite the fact that the magnitude of such orientational forces are usually very small in comparison with the energy of the transition state, the torque on the reactants at long range acts to deflect trajectories towards or away from the transition state [16].

"Heavy+light-heavy" systems such as X-HY, where X and Y are both halogen atoms, have emerged as prototypical systems to study chemical reaction dynamics at a fully quantum mechanical level [20, 21, 22, 23, 24]. The attraction of such complexes is due to the fact that they contain only 2 heavy atoms, thus simplifying the nuclear degrees of freedom, yet the corresponding electronic degrees of freedom can be quite complex. Indeed, because the unpaired electron of the free halogen atom resides in a p orbital, three potential energy surfaces are needed to fully characterize the interactions, which correspond to the three relative orientations of the p orbital with respect to HX. These surfaces become degenerate for large separations, and the coupling between the surfaces cannot be neglected [25]. Furthermore, spin-orbit coupling will also reshape the potential energy surfaces [25, 26, 27]. In this work we extend these studies by looking at a related X-HY complex, where Y is now the pseudo-halogen CN.

The reactions of halogen atoms with HCN have been the focus of extensive experimental [28, 29, 30] and theoretical study [31, 32, 33], aimed at elucidating the role of the potential energy surface in determining the associated reaction dynamics. The CN group is often regarded as a pseudo-halogen, and thus there is interest in comparing the reaction dynamics of this tetra-atomic system with the analogous X-HY (X & Y = halogen atoms) triatomic systems. Interestingly, the long range interactions between XH + CN are expected to differ significantly from X + HCN due to the threefold degeneracy associated with the ^2P ground state of halogen atoms, compared to the nondegenerate $^2\Sigma$ ground state of CN radicals, further lowering the symmetry of this hydrogen exchange reaction. Despite this, HCN is an ideal test case because the CN group is usually found to act as a single unit, but there is still considerable debate about whether or not the CN bond is a spectator to the dynamics of many different reactions [30, 34, 35]. The additional degrees of freedom that the HCN molecule presents, open up many new channels of the potential energy surface that can be explored, and the X + HCN systems have provided benchmarks for the theoretical treatment of such multi-dimensional dynamics.

The Cl-H-C-N potential energy surface has been studied experimentally from three different starting positions.

De Juan *et al.* [33] have investigated the H + ClCN → HCl + CN reaction by colliding translationally hot H atoms formed from the 248 nm photolysis of H_2S, with ClCN. This experimental arrangement prepares the reactants with 21.6 kcal mol^{-1} of collision energy, which is ∼43 kcal mol^{-1} above the energy of Cl + HCN (see Figure 2). By analyzing the nascent CN rovibrational populations, as well as the Doppler profiles of the vibrational transitions, it was proposed that CN is a spectator under these conditions, and that most of the available energy goes into HCl vibration and into translational energy of the two fragments. Sims and Smith [34] and Frost *et al.* [35] have studied the HCl(v_{HCl}) + CN(v_{CN}) → HCN + Cl reaction, and came to the conclusion that CN is also a spectator in this reaction, due to the fact that there is a negligible enhancement of the reaction rate upon exciting the CN stretching vibration. A third set of experiments were carried out by Metz *et al.* [30, 36] and Kreher *et al.* [28, 37] focusing on the reaction of translationally hot chlorine atoms with highly vibrationally excited HCN:

$$Cl + HCN(v_1, v_2, v_3) \rightarrow HCl + CN$$

Metz and coworkers showed that HCN, when prepared with either 4 quanta of CH stretch (004) or 3 quanta of CN stretch plus two quanta of CH stretch (302) react with comparable rates, and conclude that under these conditions CN "is clearly not a spectator"[84]. Another interesting observation from this work is that only 14% of the available energy was found as HCl vibration, which is surprisingly small since this is the bond that is formed in the reaction. To justify this observation an addition-elimination mechanism was proposed which involved an intermediate HClCN product, as opposed to direct collinear abstraction. Indeed, experiments in argon matrices have now proven the existence of HFCN [38, 39]. If the intermediate survived long enough in the gas-phase to permit energy redistribution, this could account for the transfer of energy from HCl(v) to CN(v). According to this mechanism the CN cannot be a simple spectator. Kreher *et al.* confirm these observations, however point out that HCN(302) does give rise to higher vibrational excitation of CN than does HCN(004), so some memory of the initial state is retained.

The global potential energy surface for Cl + HCN was first studied theoretically by de Juan *et al.* at the MP4/3-21G* level to aid in the interpretation of their experimental results [33]. Their calculations did show the existence of a covalently bound HClCN intermediate product, but the relative energies of the reactants and products showed significant discrepancies with the experimentally determined values. Harding later revisited the Cl-HCN surface at the RHF+1+2+QC/cc-pVDZ level and found the energies to be in much better agreement with experiment [32]. Although the overall topology of the two surfaces are similar, the existence of a direct HClCN → HCl + CN pathway originally proposed by de Juan *et al.* was not found by Harding. Instead, Harding points out that they most likely found the transition state for collinear abstraction. Currently an exhaustive search of the six-dimensional potential energy surface is not possible, however Harding states that this HCl elimination pathway is unlikely based on the overall topology of the potential. He finds that the transition state of the Cl + HCN → HCl + CN reaction is a collinear abstraction mechanism, and that the reaction path does not directly involve the HClCN complex, in contrast to that proposed by Metz and coworkers. Indeed the HClCN complex can be formed at energies well below the abstraction reaction, however further reaction to form HCl + CN would require surmounting barriers in excess of that for direct abstraction. In order to explain the experimental results, which clearly show vibrational excitation of the CN, Harding proposes two possible mechanisms. First, the CN stretching frequency is found in the calculations to be largely unaffected along the reaction coordinate. In contrast, the reagent CH stretch and product HCl stretches, which are initially above the CN frequency, go through a minimum at the transition state and are below the CN frequency. Because these normal modes cross the CN stretching frequency, energy could flow between these two modes along the course of the reaction. Secondly, Harding's calculations predict the existence of long-range entrance channel complexes on both sides of the abstraction transition state (Cl-HCN, HCN-Cl, and CN-HCl) which could also influence the final product state distributions.

Most recently Troya *et al.* have performed a quasiclassical trajectory study of the Cl + HCN → HCl + CN reaction [31]. Their findings are in agreement with Harding, in that the intermediate HClCN product only constitutes a minor channel (<5%) at the translational energies relevant to the previous experiments. The focus of the current study is to explore the long-range entrance channel complexes of X + HCN.

EXPERIMENTAL

A detailed description of the experimental apparatus has been given previously [40], therefore only the most salient features will be described here. Helium droplets are formed by expanding ultra-high-purity helium gas through a 5 μm nozzle which is cooled to 18-22 K. The helium stagnation pressure was maintained at 50 bar, resulting in the formation of droplets with a mean size of 2500 - 6000 atoms [41]. Halogen radicals were produced by pyrolysis [12, 42] and doped into the droplets using an effusive source while the HCN is added to the droplets downstream using a simple scattering cell. The documented growth of non-equilibrium structures in helium droplets is suggestive of a successive capture mechanism where dopants are pre-cooled before complexation occurs [8, 9, 43]. The relative timescales for species finding each

other in a droplet, to form a complex, and the rate of cooling are not precisely known. The cooling rate however must at least be competitive with coagulation in order to prevent annealing of previously formed metastable structures in the pick-up process. In much the same way, the energy gained due to the mutual interaction of two dopants must also be quickly removed and complexation will occur at low interaction energies comparable to the droplet temperature of 0.4 K. Therefore, complexes are typically trapped in a local minimum reflecting the approach geometry of the dopants; the low temperature does prevent rearrangement to the global minimum [8, 9].

The infrared light from an F-center Laser (Burleigh FCL-20) or a PPLN-OPO (Linos Photonics OS-4000) interacts with the droplet beam using a linear multipass cell, designed to increase the effective interaction length. Excitation of the dopant inside the droplet leads to evaporation of approximately 600 helium atoms from the droplet [44], which reduces the on-axis beam flux reaching a liquid helium cooled bolometer. By mechanically chopping the laser and using phase-sensitive detection, the resulting beam depletion can be recorded as a function of the laser frequency to obtain the absorption spectrum. A set of Stark electrodes was aligned orthogonal to the laser interaction so that Stark and pendular spectroscopy could be performed. The DC electric field was oriented parallel to the laser polarization yielding ΔM=0 selection rules. Details on the calibration of the electric field are given elsewhere [45]. In order to optimize conditions for the pickup of a single halogen atom, the temperature of the pyrolysis source is adjusted, monitoring the percent dissociation of the precursor by probing both the X-HCN and X_2-HCN binary complexes.

ELECTRONIC STRUCTURE CALCULATIONS

In order to characterize the precursor complexes we have calculated a two-dimensional angular potential (at the RMP2/aug-cc-pVDZ level) for HCN-Cl_2 corresponding to the two rotors being fixed within the same plane. The two angles, θ and ϕ, were stepped in increments of 10°, and the intermolecular distance R was relaxed to find its minimum in energy. The remaining geometric parameters were held fixed at the values found for separate HCN and Cl_2 optimizations, namely r_{CH} = 1.0779 Å, r_{CN}= 1.1828 Å, and r_{ClCl} = 2.3275 Å. The dissociation energy of the complex was corrected for basis set superposition error [46], and a spline interpolation was used to generate the final surface shown in Figure 1. The surface predicts a deep minimum for a linear nitrogen bound geometry (θ, ϕ) = (180, 180), and a very flat minimum around (90, 20) corresponding to a near T-shaped hydrogen bound complex. Previous gas-phase studies [47, 48, 49] have confirmed the linear geometry of the HCN-Cl_2, HCN-BrCl, and HCN-FCl complexes

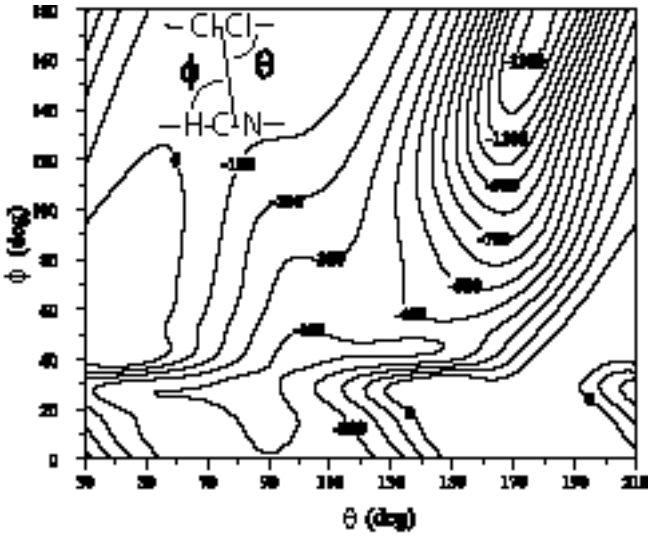

FIG. 1: A two-dimensional angular potential for HCN-Cl_2 showing two possible local minimum structures. At each point only the intermolecular distance was optimized to find its minimum in energy. Counterpoise correction was applied and the final surface generated using a bi-cubic spline interpolation algorithm. Contour lines are drawn in 100 cm^{-1} intervals. In helium droplets both isomers are observed for I_2, Br_2, and Cl_2 complexes with HCN, where as in the gas-phase only the global minimum (linear nitrogen bound) isomer has been identified [47]. Interestingly only the global minimum HCN-F_2 isomer was observed in helium.

however there has been no previous evidence (nor prediction) of a hydrogen bound isomer. Fully relaxed geometry optimizations and harmonic vibrational frequency calculations confirm that the local minimum equilibrium structure is slightly bent away from an exactly T-shaped geometry, however vibrational averaging is likely to be important due to the weak anisotropy. Exploratory calculations in which the restriction of planarity was relaxed did not result in any new minima.

As pointed out by Harding [32], the reactivity toward HCN by halogen atoms is such that two reaction products have been postulated, with the halogen covalently binding to either the carbon or nitrogen atom of HCN. Due to limitations of the basis set used and computational expense, Harding admits that the calculations performed to date are more qualitative in nature. In this section we extend these calculations to higher-levels of theory and calculate each of the F, Cl, and Br reactions so that they may be directly compared, but we only focus on the lowest energy channels including HXCN formation. To explore the relative energetics of these complexes, we have employed the G2 method [50], and the resulting stationary points, including zero-point energy, on the potential energy surface are shown graphically in Figure 2. For comparison, a few stationary points have also been calculated at the UMP2/aug-cc-pVTZ and UCCSD(T)/6-311++G(d,p) levels in addition to the G2 results, and

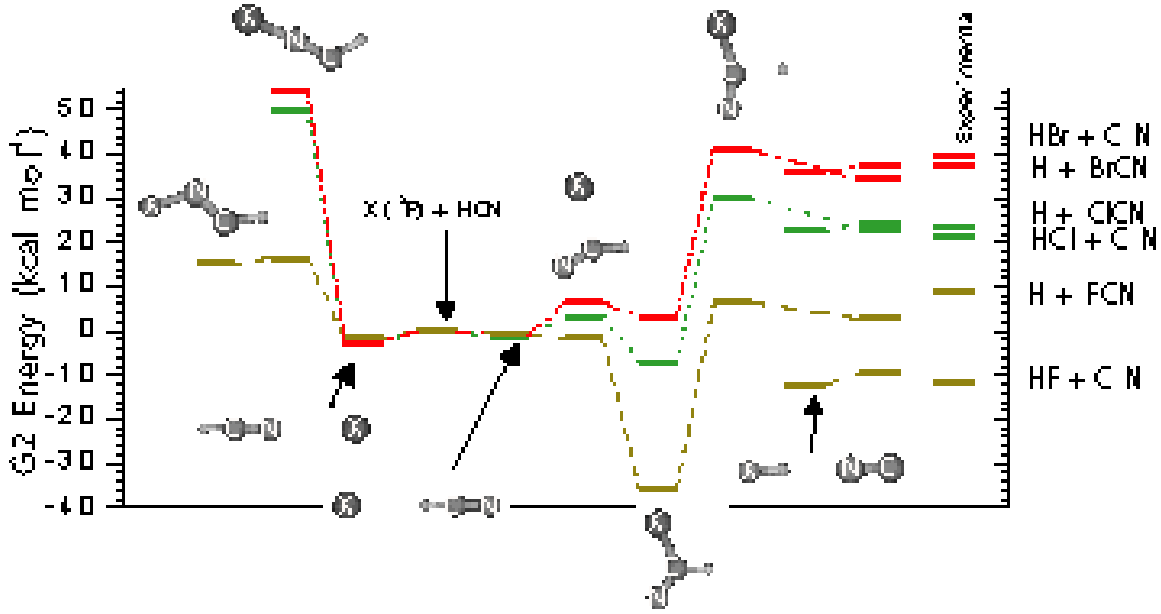

FIG. 2: Relevant stationary points of the X + HCN reactions calculated using the composite G2 method. Two reacted complexes in addition to two weakly bound entrance channel species are predicted. The HCNX products of chlorine and bromine atoms binding on the nitrogen end of HCN could not be stabilized in our calculations, however HCNCl was found in reference [32]. The experimental heats of formation for the X + HCN → HX + CN and X + HCN → H + XCN reactions are taken from reference [51]. The photon energy used to study the pre-reactive X-HCN complexes is greater than the barriers to form HXCN, suggesting that it may be possible to photo-initiate this reaction.

are summarized in Table I. The calculated enthalpies of reaction are found to be in qualitative agreement with experiment at the G2 and UCCSD(T)/6-311++G(d,p) levels of theory, however the agreement is much worse at the UMP2 level.

From Figure 2 it is clear that the X + HCN → HCNX reactions are all quite endothermic, and therefore we expect that this reaction channel will not play at role in the dynamics at 0.37 K. More relevant to the experimental conditions is the reactivity of the halogen atoms with the carbon atom of HCN. For the F + HCN reaction, a very stable HFCN intermediate product is found in the calculations. At the G2 level no barrier is predicted for this reaction, however at the UCCSD(T)/6-311++G(d,p) level the reaction barrier is 3.05 kcal mol^{-1}. Four of the six vibrational modes of this product were first observed by Andrews *et al.* [38] in an argon matrix by codepositing F_2 and HCN, and then subjecting the matrix to broadband UV photolysis. Although rotational resolution was not achieved, the observation of the CN stretching vibration at 1672 cm^{-1} indicates that the CN bond has double-bond and not triple-bond character. Of interest to the current study, the CH stretching vibration was observed at 3016 cm^{-1}. Later Misochko *et al.* confirmed Andrews observations, and assigned the two remaining vibrational modes which were not observed previously [39]. Experimental evidence for a pre-reactive X+HCN complex or HClCN however is still lacking.

Harding's calculations on Cl+HCN are given in Table I, and in general, agree well with our current calculations. G2 (UCCSD(T)) calculations predict that the reaction of a chlorine atom with the carbon of HCN is exothermic by -7.07 (-3.41) kcal mol^{-1} , and that the barrier height is 3.30 (6.97) kcal mol^{-1} . For bromine atoms, the reaction to form HBrCN is predicted to be endothermic at the G2 level of theory. Since the CH stretching vibration of the entrance channel complexes has a higher frequency than the barrier to form HXCN, it may be possible to photo-initiate the reaction starting from the entrance channel.

While the above calculations give us an overview of the reaction energetics for the halogen atom - HCN reactions, we are particularly interested in the topology of the surface around the entrance channel. For instance, it appears that HCN+X might be most reactive in a T-shaped arrangement, so the long-range orientational effects of the potential may be very important in determining the reaction dynamics. To begin to answer these questions we have calculated three-dimensional (R, θ, r_{CH}) non-relativistic adiabatic potential energy surfaces for Br + HCN and Cl + HCN at the RCCSD(T)/aug-cc-pVDZ+{332} level of theory. The transformation of these surfaces to include spin-orbit coupling, and the calculation of the resulting bound states is being performed in collaboration with the group of van der Avoird, and details on these results will be presented elsewhere [52]. In order to gain insight into our experimental results, we

	G2	UCCSD(T) 6-311++G(d,p)	UMP2 aug-cc-pVTZ	Experimental (ΔH)	Harding [32] RHF+1+2+QC/cc-pVDZ
Cl (F) + HCN	0.0	0.0	0.0	0.0	0.0
T.S.	3.30 (-1.70)	6.97 (3.05)	-[a]	-	8.2
HClCN (HFCN)	-7.07 (-35.83)	-3.41 (-28.44)	4.91 (-27.18)	-	-2.2
HCNCl (HCNF)	-[a] (15.32)	-[a] (22.60)	-[a] (26.86)	-	27.9
HCl (HF) + CN	24.21 (-9.45)	25.37 (-6.54)	42.90 (6.18)	21.41 (-11.58)	25.9
ClCN (FCN) + H	23.11 (2.71)	26.80 (9.17)	19.03 (-3.03)	23.45 (9.26)	28.8

[a] Could not be stabilized in the geometry optimization.

TABLE I: A summary of the calculated energetics of the Cl (F) + HCN reactions including zero-point energy. T.S. corresponds to the transition state of the reaction with the carbon atom of HCN to form HXCN. The experimentally determined heats of reaction (ΔH) are also shown for reference [51]. One can see that while the G2 and UCCSD(T) methods predict the enthalpies quite well, the UMP2 method shows much larger deviations. A graphical representation of these energies is shown in Figure 2 for the G2 calculations. Previous calculations by Harding for Cl + HCN are also given for reference.

will focus our attention on the qualitative features of a 2D slice (r_{CH} = 1.0655 Å) from our 3D non-relativistic adiabatic potentials, which are shown in Figure 3 for Br + HCN. The incorporation of the dimension corresponding to the CH bond length of HCN (r_{CH}) will lend insight into the change of the 2D potentials upon vibrational excitation of HCN (ν_1).

Calculations were performed using MOLPRO [53], employing Jacobi coordinates, R and θ, and restricting the electronic wavefunction to C_s symmetry, which gives rise to the 1A', 2A', and 1A" surfaces, corresponding to the three relative orientations of the unpaired orbital of the halogen atom with respect to HCN. A set of uncontracted mid-bond functions with exponents sp: 0.9, 0.3, 0.1, and d: 0.6, 0.2 (denoted as {332}) have been added to the aug-cc-pVDZ basis set and were placed at the midpoint between the halogen atom and the HCN nuclear center of mass [54, 55]. For the plots shown in Figure 3, R and θ have been incremented by 0.1 Å and 10° respectively. The r_{CH} and r_{CN} bond lengths of HCN were fixed at 1.0655 and 1.1532 Å respectively. Basis set superposition error has been accounted for by performing counterpoise correction [46], and a spline interpolation used to smooth the surface. As noted by Fishchuk *et al.* for Cl-HF [56], there is some choice in how counterpoise correction is applied due to the two A' states of the free halogen atom. Our procedure is the same as that reported for Cl-HF, in that the lowest RCCSD(T) energy of the free halogen atom was subtracted from both A' dimer energies, which preserves the double degeneracy of the Π state for both linear geometries. The nitrogen bound (HCN-X) geometry corresponds to $\theta = 0°$.

The surfaces clearly show that both linear geometries have stable minima, with well depths of -810 and -401 cm^{-1} for the HCN-Br and Br-HCN isomers respectively. The isomerization barrier connecting Br-HCN to HCN-Br is found to be only 90 cm^{-1} (neglecting zero-point effects). At $\theta = 0$, the 1A" and 2A' surfaces correlate with the doubly degenerate $^2\Pi$ state, where as for $\theta = 180$, it is the 1A' and 1A" surfaces. The ground electronic state of the HCN-Br isomer is $^2\Sigma$ and for Br-HCN it is $^2\Pi$ in agreement with that found by Harding [32]. These symmetries illustrate that the unpaired orbital of the halogen atom is along the axis of the molecule for $^2\Sigma$, while it is perpendicular to the molecular axis for $^2\Pi$. These different electronic symmetries are determined by electrostatic interactions of this dipole-quadrupole system. In the linear nitrogen bound complex the negative end of the HCN dipole will want to approach the positive p-hole created by the unpaired orbital, thus orienting the unpaired orbital on the molecular axis. When the positive end of the HCN dipole approaches the Br, the positive p-hole will be repelled, and orient itself perpendicular to the molecular axis, resulting in a Π ground state.

Fully relaxed geometry optimizations, at the RMP2 level, were also undertaken for each of these stable structures to generate dipole moments and scaled harmonic frequencies to compare with our experiment, which are summarized in Table II. Note that vibrational frequencies could not be calculated for the basis sets which include mid-bond functions, so we have instead used the aug-cc-pVTZ basis set. Calculations for iodine containing complexes employed the aug-cc-pVTZ-PP [57] pseudo-potential for the iodine atom. One can see that while the binding energy for Br-HCN is in very good agreement with the 2D surfaces (399.5 cm^{-1} at the RMP2/aug-cc-pVTZ level compared with the 2D RCCSD(T)/aug-cc-pVDZ+{332} result of 401 cm^{-1}), the differences found for HCN-Br are somewhat greater (910 vs. 810 cm^{-1}).

Relativistic - adiabatic potential energy surfaces

The effects of spin-orbit coupling on reshaping the potential energy surface is well documented [54, 58] and in order to make detailed comparisons with our experiment we must incorporate it. To include spin-orbit coupling

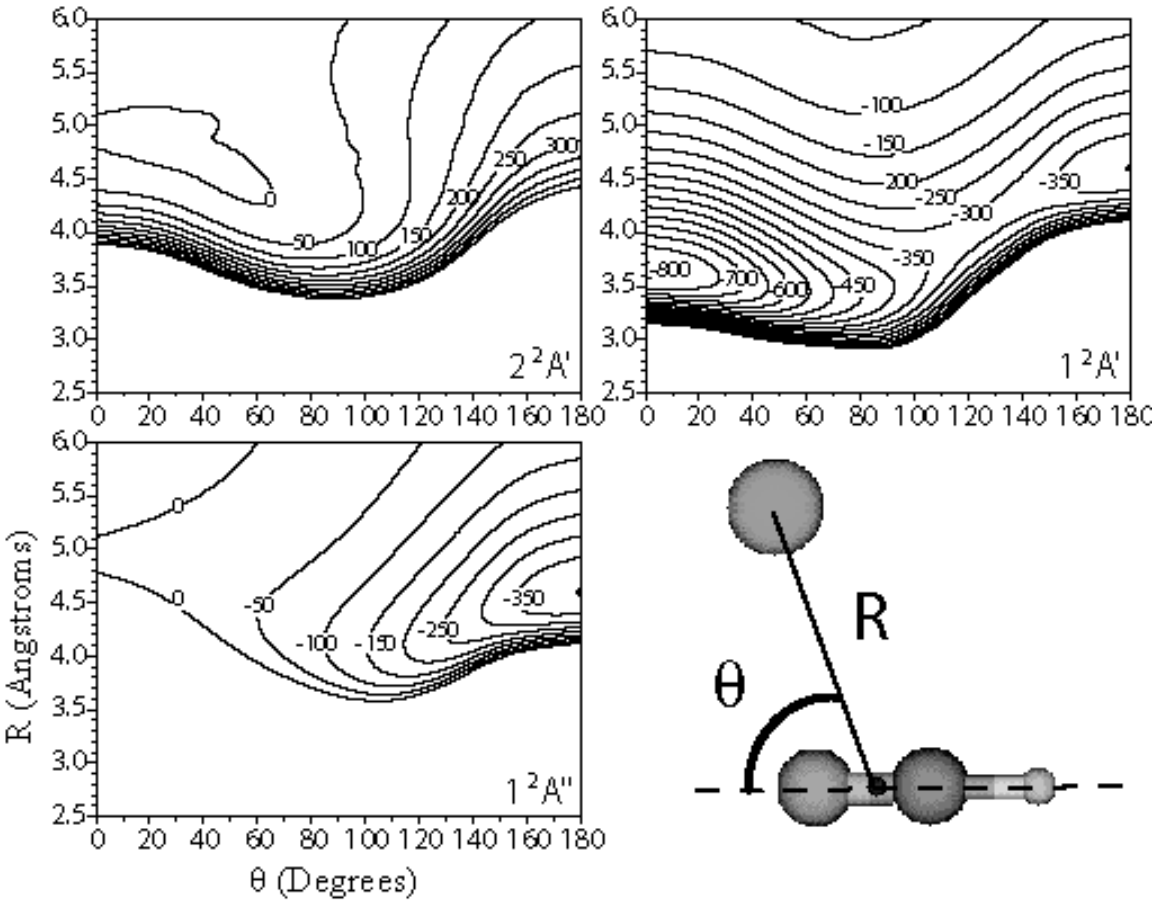

FIG. 3: The three non-relativistic adiabatic potential energy surfaces for HCN + Br calculated at the RCCSD(T)/aug-cc-pVDZ+{332} level. Contour lines are drawn in 50 cm^{-1} intervals. The surfaces predict both linear structures to be minima.

RMP2 aug-cc-pVTZ	HCN-F (F-HCN)	HCN-Cl (Cl-HCN)	HCN-Br (Br-HCN)	HCN-I (ECP) (I-HCN (ECP))
D_e (cm^{-1})	405.2	834.3	909.8	935.1
	(189.0)	(359.9)	(399.5)	(429.4)
$\nu_{harmonic}$ (cm^{-1})	-[a]	3464.21	3463.11	-[a]
	-[a]	(3443.85)	(3433.52)	(3430.88)
ν_{scaled} (cm^{-1})	-	3309.11	3308.06	-
	-	(3291.66)	(3281.78)	(3279.26)
R (Å)	3.240	3.416	3.542	3.726
	(4.015)	(4.342)	(4.475)	(4.670)
B (cm^{-1})	0.1310	0.0885	0.0636	0.0525
	(0.0881)	(0.0561)	(0.0405)	(0.0339)
μ (D)	3.24	3.66	3.77	3.91
	(3.18)	(3.40)	(3.47)	(3.58)

[a]Tight geometry convergence was achieved but imaginary frequencies were calculated

TABLE II: Computed properties of the HCN-X (X-HCN) isomers at the RMP2/aug-cc-pVTZ level. The calculations for iodine incorporate a small core relativistic pseudo-potential (aug-cc-pVTZ-PP) in which 28 core electrons were replaced with the ECP [57]. Binding energies have been corrected for BSSE [46]. Harmonic frequencies have been scaled by a factor of 0.9552, which is obtained by comparing a HCN calculation at this level to the corresponding experimental helium droplet band origin. R, is the X-HCN center of mass distance.

for the linear geometries (1D slices) of our 2D *ab initio* potentials we take note of the operator form of the spin-orbit Hamiltonian:

$$\begin{aligned} H^{so} &= A\mathbf{L}\cdot\mathbf{S} \\ &= A(L_zS_z + \frac{L^+S^- + L^-S^+}{2}) \end{aligned}$$

The spin-orbit coupling constant, A, is -269.3, -587.3, -2457, and -5068 cm^{-1} for F, Cl, Br, and I, respectively [59]. Note that the negative sign for A illustrates that the $^2P_{3/2}$ state lies below the $^2P_{1/2}$ state in the free atoms. We make the approximation that the spin-orbit coupling is independent of the geometry of the complex, and remains that of the isolated atom. That this approximation is valid for the long-range part of our potentials is justified because the electron-nuclei interaction scales as $\langle\frac{1}{r^3}\rangle$[59], and therefore the inner lobes of the orbitals are more heavily weighted, which are expected to be only slightly perturbed by the relatively weak van der Waals interaction. Recent calculations on $O(^3P)$ + HCl by Rode *et al.* [60] have examined the validity of this approximation by explicit calculation of the spin-orbit matrix elements using the Breit-Pauli operator [61]. Their results indicate that for internuclear distances similar to the van der Waals separation the spin-orbit coupling is not substantially affected.

The diagonal term of the spin-orbit Hamiltonian (L_zS_z) gives the $^2\Pi_{1/2}$ and $^2\Pi_{3/2}$ potentials as $^2\Pi \mp \frac{A}{2}$, while the $^2\Sigma$ potential is simply $^2\Sigma_{1/2}$. This is illustrated by plugging in the eigenvalues of the L_z and S_z operators, namely $\Lambda = 1$ and $\Sigma = +1/2$ for the $^2\Pi_{3/2}$ state and $\Lambda = 0$ and $\Sigma = |1/2|$ for the $^2\Sigma_{1/2}$ state. The off-diagonal spin-orbit term ($L^\pm S^\mp$) couples the $^2\Pi_{1/2}$ state with the $^2\Sigma_{1/2}$ state and has the following form [59]:

$$\left\langle {}^2\Pi_{1/2}|\frac{A}{2}L^+S^-|{}^2\Sigma_{1/2}\right\rangle = 2^{1/2}(A/2)$$

To derive the relativistic adiabatic potentials we set up a R dependent 2 × 2 matrix for the $\Omega = 1/2$ states, set the diagonal elements to the energies from the *ab initio* calculation, and the off-diagonal elements to $2^{1/2}(\frac{A}{2})$, and diagonalize the matrix numerically to get its eigenvalues and eigenvectors. For this simple two level system, the potentials (eigenvalues) are given by:

$$\begin{aligned} {}^2\Sigma_{1/2} &= a^2({}^2\Pi - \frac{A}{2}) + (1-a^2)({}^2\Sigma) \\ {}^2\Pi_{1/2} &= a^2({}^2\Sigma) + (1-a^2)({}^2\Pi - \frac{A}{2}) \end{aligned}$$

where a is an R dependent mixing coefficient. The remaining $^2\Pi_{3/2}$ state is simply $^2\Pi + \frac{A}{2}$. The diagonalized relativistic and non-relativistic adiabatic potentials are shown in Figure 4. At long range, where the Σ and Π states are nearly degenerate, the $^2\Sigma_{1/2}$ state is pushed lower in energy compared to $^2\Sigma$ while the $^2\Pi_{1/2}$ is pushed to higher energies compared to $^2\Pi - A/2$ due to the coupling. In the limit of R → ∞ , the $^2\Pi_{3/2}$ and $^2\Sigma_{1/2}$ states converge and the separation between $^2\Pi_{1/2}$ and $^2\Pi_{3/2}$ becomes (3/2)A, or that observed in the free atom. The bound states of these potentials were calculated numerically using the program Level [62] and the binding energies, rotational constants, and the van der Waals stretching frequencies are summarized in Table III. To estimate the effects of CH stretching of HCN on the potentials, computations were also performed in which the HCN geometry was constrained to have a CH bond length of r_{CH} = 1.09 Å, which is close to the vibrationally averaged bond length for the $v = 1$ state. In general, the excitation of HCN results in a slight increase in the binding energy of the complex which we attribute to an increased dipole - quadrupole interaction.

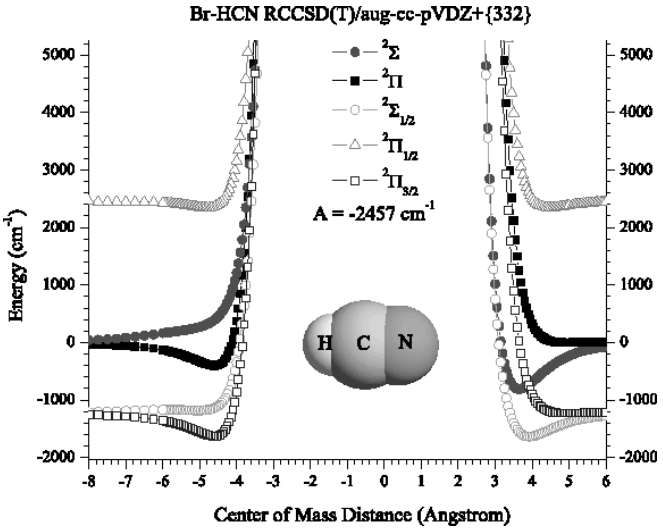

FIG. 4: Relativistic and non-relativistic adiabatic potential energy curves for the HCN-Br complex derived from the *ab initio* results. See text for details.

As noted above, spin-orbit coupling can strongly influence the potentials, and indeed the dissociation energy of the HCN-Br ($^2\Sigma_{1/2}$) complex is much smaller than in the non-relativistic calculation (383 vs 773 cm^{-1}). The spin-orbit interaction is even strong enough to create a bound state in the upper $^2\Pi_{1/2}$ well, despite the fact that the $^2\Pi$ state is purely repulsive. But since this state correlates with the excited spin-orbit component of the atom, we would not expect this isomer to be produced in helium. For the hydrogen bound isomer, the ground state is predicted to be $^2\Pi_{3/2}$. Since this potential is not distorted from the non-relativistic $^2\Pi$, we expect that the nonrelativistic *ab initio* calculations for this isomer should be sufficient to compare with experiment. This may not be the case for the HCN-X complexes, and thus the nonrelativistic *ab initio* results should be interpreted with caution. After inclusion of the spin-orbit coupling,

Constant (cm^{-1})		Br-HCN	
HCN $v_1 = 0$ ($v_1 = 1$)	$^2\Pi$	$^2\Pi_{1/2}$	$^2\Sigma_{1/2}$
D_0	376.43 (390.04)	[a]	[a]
B_0	0.03893 (0.03893)	[a]	[a]
ν_{vdws}	47.37 (48.36)	[a]	[a]
		HCN-Br	
	$^2\Sigma$	$^2\Sigma_{1/2}$	$^2\Pi_{1/2}$
D_0	773.23 (775.89)	383.33 (384.94)	111.24
B_0	0.06233 (0.06235)	0.05379 (0.05382)	0.04051
ν_{vdws}	69.71 (69.84)	47.88 (47.97)	26.91

[a] No bound states found

TABLE III: A summary of the computed properties for the HCN-Br and Br-HCN isomers from bound state calculations on one-dimensional relativistic adiabatic potentials. Note that the computed bound states for the $^2\Pi_{3/2}$ state are the same as those for the non-relativistic $^2\Pi$ state.

we find that both isomers for bromine are now nearly isoenergetic. The smaller spin-orbit coupling constant for chlorine atoms allows the HCN-Cl complex to remain the global minimum. We look forward to the results of including spin-orbit coupling into our 2D and 3D surfaces as it will be particularly interesting to investigate how the isomerization barrier is effected. Table IV collects the molecular parameters derived from the bound states for the HCN-Cl, HCN-Br, and HCN-I complexes.

THE HCN-X_2 COMPLEXES

Given that previous experimental [48, 49] studies have shown that halogen molecules bind to the nitrogen end of HCN, the search for the HCN-X_2 complexes was straightforward given the weak perturbation on the CH stretching frequency. Pendular survey scans for Br_2, Cl_2, and F_2 + HCN are shown in Figure 5, and the new peaks are labeled according to their gas dependence. The smooth variation in frequency shifts is telling of the magnitude of the interactions. Figure 5 also shows the resulting zero-field spectra for the HCN-Br_2, HCN-Cl_2, and HCN-F_2 binary complexes. Molecular iodine complexes with HCN were also observed but are not shown in the figure. Due to the fact that our calculations predict that each complex is linear, in accordance with the previous microwave results [48, 49], the Q branches in the bromine and chlorine spectra are clearly unexpected. At this time we leave their explanation to a future study. We only postulate here that an impurity complex could be overlapping the band, or that the helium interaction with these species is quite strong, due to the increased polarizability compared to F_2, and thus more strongly influences the spectra [63, 64]. A similar effect in HCN trimer, another linear complex with a Q branch, has been treated theoretically, and the Q branch was found to result from the thermal excitation of the droplet in the first few solvation shells, which rotates more rigidly about the a-axis [64]. Possibly these molecular halogen complexes exhibit similar behavior.

Longer pendular scans were also carried out to search the hydrogen bonded frequency region, given the prediction of a second, nearly T-shaped, minimum. Indeed, as shown in Figure 6 for the case of bromine, a strong peak is observed at 3286.14 cm^{-1} which we assign to such a complex. Our assignment is based on pick-up cell pressure dependence measurements (optimized 1:1 with HCN-Br_2), scaled harmonic frequency calculations, rotational band contour analysis, and pyrolysis source temperature dependence. Hydrogen bonded complexes between molecular iodine and chlorine with HCN were also observed whereas the corresponding isomer of fluorine was not. The survey scans for all cases are shown in Figure 6 as downward going peaks. The fact that a hydrogen bound F_2-HCN isomer is not formed might be attributed to a smaller well depth, due to the smaller polarizability of fluorine compared with chlorine, bromine, and iodine, and larger zero-point energy effects allowing it to convert back to the global minimum linear nitrogen bound geometry, which is observed. The infrared spectra for these complexes taken under field-free conditions will be presented elsewhere. The dotted lines in Figure 6 illustrate the almost perfect linear scaling of the band origins for both the free stretch and the hydrogen bonded complexes.

THE Br-HCN AND I-HCN COMPLEXES

Br-HCN

Given the identification of the precursor complexes, we are now in a position to heat the pyrolysis source to produce the corresponding atoms. As in our previous study of the X-HF systems, at sufficiently high pyrolysis

Constant (cm^{-1})	HCN-^{35}Cl		HCN-^{79}Br		HCN-I[a]	
v=0 (v=1)	$^2\Sigma$	$^2\Sigma_{1/2}$	$^2\Sigma$	$^2\Sigma_{1/2}$	$^2\Sigma$	$^2\Sigma_{1/2}$
D_0	687.65 (689.98)	476.78 (478.86)	773.23 (775.89)	383.33 (384.94)	781.08	375.61 (377.24)
B_0	0.08784 (0.08786)	0.08478 (0.08482)	0.06233 (0.06235)	0.05379 (0.05382)	0.05038	0.04245 (0.04247)
ν_{vdws}	75.85 (75.98)	64.23 (63.53)	69.71 (69.84)	47.88 (47.97)	62.37	43.44 (43.52)
A	-	-587.3	-	-2457	-	-5068

[a]This calculation was performed with the aug-cc-pVDZPP+{332} basis set [57].

TABLE IV: A summary of the molecular parameters derived from the bound states of one-dimensional potential energy surfaces (see text). A is the atomic spin-orbit coupling constant used in the calculations and ν_{vdws} is the van der Waals stretching frequency, defined as the energy separation between the two lowest calculated bound states. For the "$v = 1$" calculations, the CH bond length was fixed at 1.09 Å (compared to 1.0655 Å for $v = 0$) in order to estimate the effects of vibrational excitation of the HCN. Note that the corresponding calculations for the X-HCN isomers are not presented since the ground electronic state of these complexes is $^2\Pi_{3/2}$, which does not experience a first order coupling with the $^2\Sigma$ state, and so the molecular parameters are the same as those found in a standard *ab initio* calculation presented in Table II.

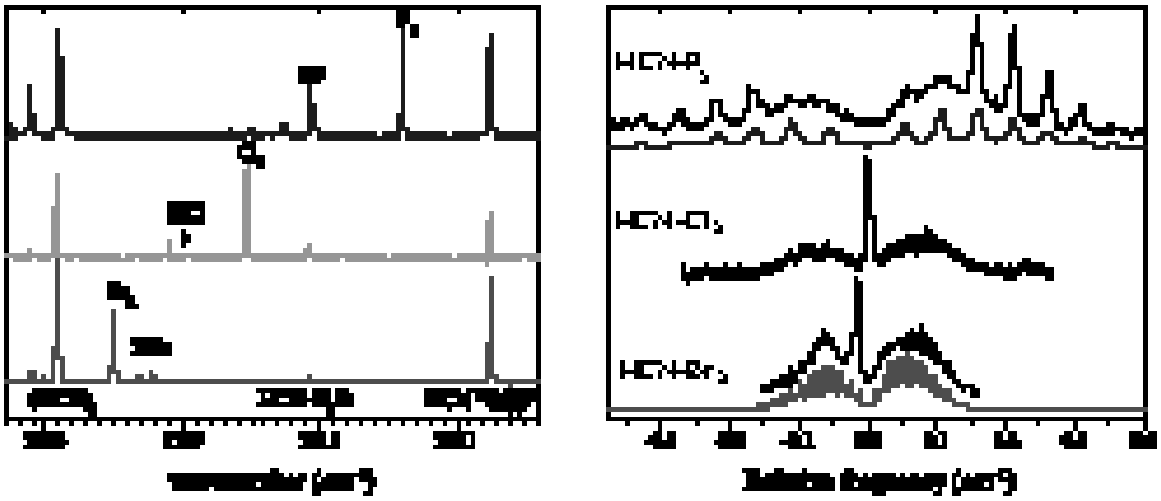

FIG. 5: Pendular survey scans showing the formation of HCN-X_2 molecular complexes (left panel) and their corresponding field-free spectra (right panel). Significant perturbations are observed in the HCN-Br_2 and HCN-Cl_2 spectra (leading to the otherwise forbidden Q branch) which we ascribe to a helium droplet interaction.

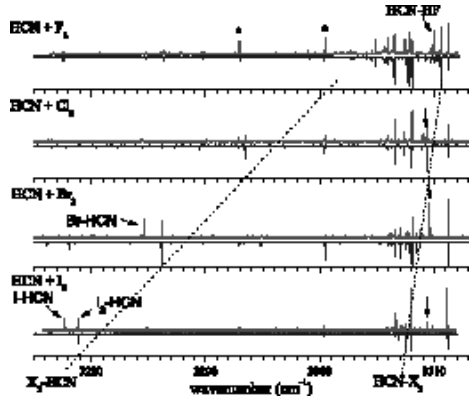

FIG. 6: Pendular survey scans revealing the pyrolysis source temperature dependence (upward peaks are with a hot source, downward peaks are with a cold source) on the corresponding HCN + halogen experiment. The scans show peaks which we identify as molecular and atomic halogens complexed with HCN. The dotted lines are drawn to guide the eye, exemplifying the linear scaling of the molecular halogen complex frequency shifts. The peaks labeled with an asterisk are known impurities. Vertical arrows point to the peaks which correspond to free CH stretch HCN-X complexes.

source temperatures the signal levels associated with the molecular halogen complexes decrease, due to dissociation into atoms, and a complementary set of peaks grow in. The pendular survey scans performed with a hot pyrolysis source are shown in Figure 6, as upward going peaks. Each scan was taken at the appropriate pyrolysis source temperature for the dissociation of that particular precursor. Concentrating on the bromine spectra, two new peaks are observed with the hot source, namely at 3309.55 and 3284.61 cm^{-1}. Based on the frequency shifts of these two bands it is already apparent that both linear isomers of HCN - Br may be formed, with the hydrogen bonded isomer giving a much larger redshift on the CH stretching frequency than the corresponding nitrogen bonded isomer. We choose to first focus on the peak we preliminarily assign to a hydrogen bonded complex since a direct comparison can be made with the corresponding X-HF complexes studied previously [12].

A field-free spectrum of the pendular peak centered at 3284.61 cm^{-1} is shown in Figure 7(A). Again this band is only observed under conditions appropriate for bromine atom pickup. In agreement with that found for the Br-HF complex, P, Q, and R branches are observed, consistent with a linear complex in a Π ground electronic state. For Br-HF a distinct 5B gap was observed between the Q branch transitions and those arising from the first P and R branch transitions which confirmed the ground state is $^2\Pi_{3/2}$, consistent with the fact that the ground state of free bromine atoms is $^2P_{3/2}$. The smaller rotational constant of Br-HCN however, makes these gaps in the spectra more obscure, but due to the predicted weak coupling of the spin-orbit interaction upon complexation,

Constant	Br-HCN	I-HCN
ν_0 (cm^{-1})	3284.61(1)	3277.79(1)
B (cm^{-1})	0.0151(5)	0.0120(5)
D (cm^{-1})	1.5×10^{-4}	1.0×10^{-4}
[aΛ + (b+c)Σ] (cm^{-1})	0.04(1)	0.04(1)

TABLE V: A summary of the experimental parameters for the linear hydrogen bound X-HCN complexes obtained from a fit to the field-free spectra.

we can say with confidence that this is also $^2\Pi_{3/2}$ band in analogy with Br-HF. A fit to the spectrum adopting the same Hamiltonian as used for Br-HF is shown in Figure 7(B). A nuclear magnetic hyperfine perturbation of the form [65]:

$$H' = a\Lambda(I \cdot k) + b(I \cdot S) + c(I \cdot k)(S \cdot k)$$

was also included in the Hamiltonian to reproduce the relative intensities of the P, Q, and R branches, in agreement with that observed for Br-HF, although here we do not resolve the individual hyperfine transitions. The $(I \cdot k)$ term represents the coupling of the nuclear spin with the axial magnetic field of the molecule, which is proportional to Λ, $(I \cdot S)$ is the direct coupling of the nuclear and electronic spin angular momenta, and $(I \cdot k)(S \cdot k)$ is a second order interaction of the nuclear and electronic spins due to both of their projections on the molecular axis. Assuming Hund's case (a), the expression for the interaction energy is:

$$W = [a\Lambda + (b+c)\Sigma]\frac{\Omega}{J(J+1)}I \cdot J$$

where

$$I \cdot J = \frac{F(F+1) - J(J+1) - I(I+1)}{2}$$

Note that the quantum number representing nuclear spin (I) equals 3/2 for bromine atoms, and F (the quantum number representing the total angular momentum including nuclear spin) is the coupling of J and I. The relative transition intensities were calculated using spherical tensor matrix elements similar to those already reported for the Stark effect for X-HF [12, 66], and a Boltzmann distribution for the rotational state population at 0.37 K. Individual transitions are convoluted with a 0.024 cm^{-1} Lorentzian lineshape function which was also varied to obtain the best fit. The spectroscopic constants (ν, B, D, and [aΛ+ (b+c)Σ]) resulting from the fit are summarized in Table V.

The experimental (helium) rotational constant is a factor of 2.7 smaller than that predicted from our *ab initio* calculations due to the fact that some of the helium follows the rotational motion of the molecule, thus adding to the complexes moment of inertial [67]. This magnitude

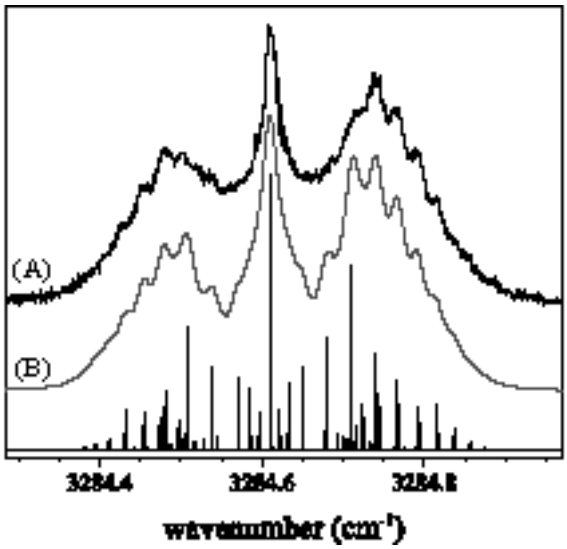

FIG. 7: (A) The rotationally resolved spectrum of the hydrogen bound Br-HCN isomer recorded under electric field-free conditions. The band shape is consistent with a $^2\Pi_{3/2}$ ground electronic state which is in agreement with theoretical predictions. The simulation (B) includes a nuclear magnetic hyperfine interaction (I=3/2 for bromine) due to the large magnetic moment of the bromine nucleus. A Lorentzian linewidth of 0.024 cm^{-1} was used for the simulation.

of reduction is in good agreement with that observed for many other systems. The fact that the rotational constant of Br-HCN is reduced by a factor of 2.7 while the rotational constant of Br-HF is reduced by a factor of 2.2 is also in agreement that the rotational constant reduction factor is usually proportional to the magnitude of the B value in this range [67]. For Cl-HF, the experimental vibrational frequencies have provided a very precise benchmark for theoretical calculations [56, 68], and it will be interesting to compare similar calculations for X-HCN [52]. The scaled harmonic vibrational frequency (RMP2/aug-cc-pVTZ) for this isomer is 3281.78 cm^{-1}, in good agreement with that observed (3284.61 cm^{-1}).

The vibrational frequencies of helium solvated rotors are typically very close to the gas phase values, owing to the weak interactions of the solvent, thus in general allowing a direct comparison with theory. A systematic increase in the vibrational red-shifts of complexes exhibiting linear hydrogen bonds has been observed however [67]. While a fully quantitative theory for this observation is still lacking, such an effect can be qualitatively understood by the fact that the helium will act to reduce the amplitude of vibrational averaging, therefore making the hydrogen bond more linear, and thus stronger, leading to a greater frequency shift. A second contribution to the observed red-shift is also expected to arise from a polarization effect due to the transition dipole moment of HCN, giving rise to dipole - induced dipole interactions with the solvent, which further lowers the energy of excited state with respect to the ground state. By fitting the enhancement of the frequency shift (helium - gas phase origin (Y)) versus the absolute magnitude of the shift observed in helium (complex - monomer origin (X)) for a database of 13 complexes observed both in helium and the gas phase, we have developed an empirical correction factor for the influence of the helium on the "gas-phase" band origin (in cm^{-1}):

$$Y = 1.822 + 0.03655X \quad (1)$$

The standard deviation of Y is 1.2 cm^{-1}. See Figure 21 of reference [67] for a plot of the experimental data points. Correcting for the helium induced shift one arrives at a predicted gas-phase origin of 3287.40 cm^{-1}. Although this makes the agreement with the scaled harmonic frequency somewhat worse, it is probably within the error of the *ab initio* calculations, and we await an estimate for the vibrational frequency from bound state calculations.

I-HCN

A similar study was carried out for the I-HCN complex, the infrared field-free spectrum being shown in Figure 8(A). The fit to the spectrum includes the hyperfine effects discussed above, however, I = 5/2 for iodine. The molecular constants derived from the fit are given in Table V. Here again the experimental rotational constant is consistent with the *ab initio* calculations, corresponding to a ratio of 2.83. The frequency shift from HCN monomer is measured to be -33.41 cm^{-1} (estimated gas-phase value using Equation 1: -30.37 cm^{-1}), in excellent agreement with the calculations employing the ECP (-31.94 cm^{-1}). The nuclear magnetic hyperfine constant used in the fit is the same as for Br-HCN, namely 0.04 cm^{-1}. This is reasonable given that the magnetic moments for the atoms are quite similar [69, 70].

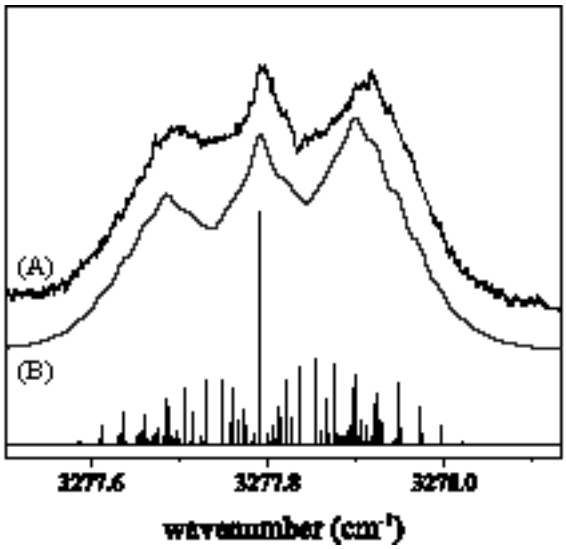

FIG. 8: (A) A field-free spectrum of the I-HCN complex in helium droplets. The fit to the spectrum (B), which includes the effects of nuclear hyperfine (I=5/2 for iodine), was used to derive the spectroscopic constants given in Table V. A Lorentzian linewidth of 0.03 cm^{-1} was used for the simulation.

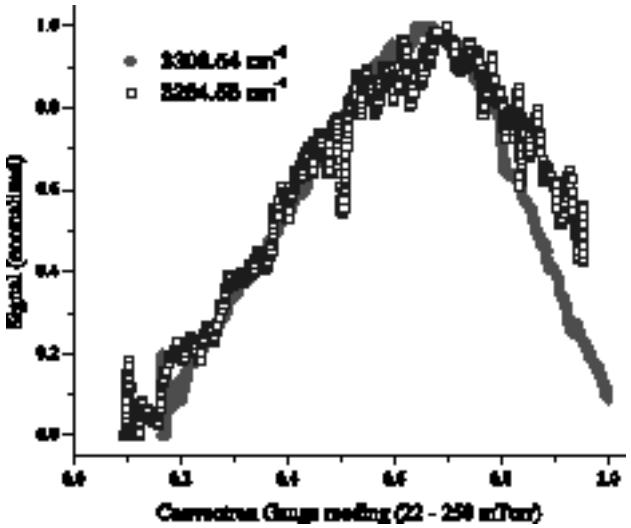

FIG. 9: Br-HCN and HCN-Br pyrolysis source pressure dependence measurements which aid in the determination that both observed bands are due to 1:1 complexes.

From the survey scans of Figure 6, peaks corresponding to the analogous Cl-HCN and F-HCN complexes are not observed. This is in contrast to the free stretch region where a new peak is observed for the HCN + Cl case, which will be discussed below.

THE HCN-Br AND HCN-I COMPLEXES

HCN-Br

We now turn our attention to the second set of new pendular peaks that grow in under the appropriate conditions for halogen atom pickup, namely those that exhibit a much smaller red-shift from HCN monomer. In the HCN + Br pendular survey scan (Figure 6), a peak is observed at 3309.55 cm^{-1} which is red-shifted from HCN monomer by -1.65 cm^{-1}, in qualitative agreement with the calculations for a nitrogen bound HCN-Br isomer (-3.14 cm^{-1} at the RMP2/aug-cc-pVTZ level). Because the ground electronic state of this complex is predicted to be $^2\Sigma_{1/2}$, spin-orbit coupling could be important in this system, and thus harmonic frequency calculations (which are performed on the $^2\Sigma$ surface) are only semi-quantitative. From our 1D PES's which include spin-orbit coupling, we find that the binding energy of the complex is increased by 1.61 cm^{-1} upon "vibrational excitation" of the HCN. Neglecting dynamical coupling of the different dimensions of the PES, this increase in the binding energy upon excitation necessitates a red-shift in the vibrational frequency of equal value, in excellent agreement with that observed, namely -1.65 cm^{-1}. Such excellent agreement could be fortuitous, and it will be interesting to compare this estimate with the results from higher dimensional calculations. An analogous comparison between the v_{CH}=0 and v_{CH}=1 bound states for the non-relativistic curves gives a frequency shift of -2.66 cm^{-1}, which is in much poorer agreement with experiment.

The pick-up of dopants by helium droplets is a statistical process, and the signal intensity as a function of dopant pressure, a Pick-Up Cell (PUC) pressure dependence curve, is given by a poisson distribution weighted by the droplet size distribution for a given set of source conditions [67]. PUC curves are a valuable characterization tool because higher order clusters can easily be distinguished by their optimum pressure. For our pyrolysis measurements, the pick-up zone is rather ill defined, however the optimum molecular halogen pressure upstream of the pyrolysis region could be used to aid in the determination of this new band to a second isomer of bromine atoms complexed with HCN. A pressure gauge was added to the pyrolysis source and the resulting pressure dependence curves for the two peaks at 3309.54 and 3284.55 cm^{-1} are shown in Figure 9. Both bands are found to have exactly the same bromine pressure dependence, confirming that this new band at 3309.54 cm^{-1} is also due to a 1:1 complex.

The field-free and Stark spectra for this band are shown in Figure 10(A) and (C). The band shape is consistent with that of a linear rotor in a $^2\Sigma$ electronic state, as predicted by our earlier electrostatic arguments. In the field-free spectrum there appears to be fine structure, most notably as a splitting in the low rotational transitions. We tentatively ascribe this splitting to an interaction of the (relativistic) $^2\Sigma_{1/2}$ and $^2\Pi_{1/2}$ states, which

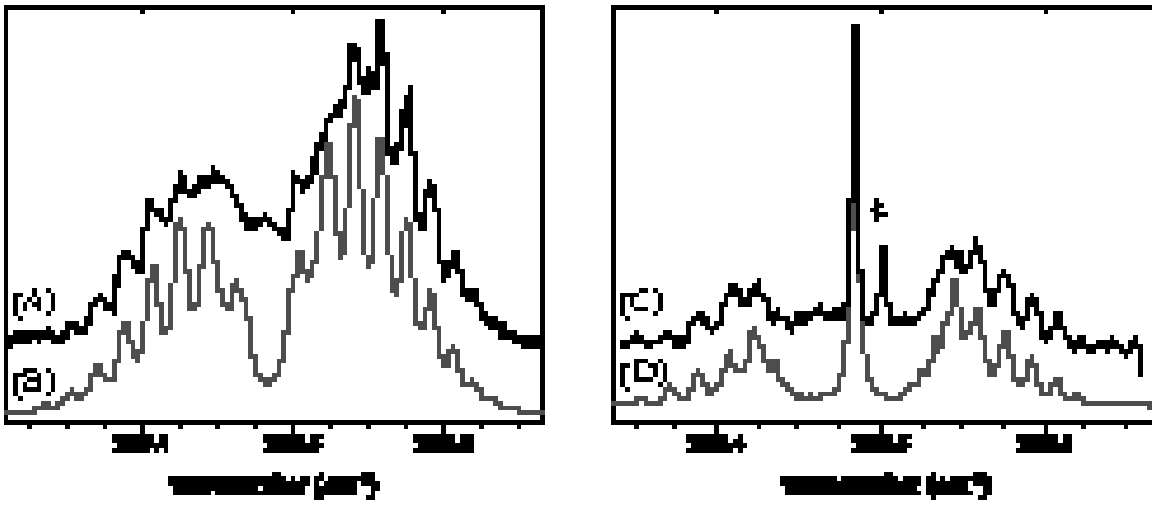

FIG. 10: (Left panel) (A) An infrared field-free spectrum for the CH stretching vibration of the HCN-Br complex. Fine structure is observed which we preliminarily assign to a parity splitting induced by spin-orbit coupling of the $^2\Sigma_{1/2}$ and $^2\Pi_{1/2}$ states of the complex. A simulation of the band is also shown (B) which includes the effects of spin-orbit coupling. (Right panel) (C) The corresponding Stark spectrum for the HCN-Br complex recorded at an electric field strength of 2.25 kV cm^{-1}. The peak marked with an asterix is assumed to be related to an impurity complex. Lorentzian linewidths of 0.025 and 0.01 cm^{-1} were used for fitting the field free and Stark spectra respectively.

are coupled by the off-diagonal spin-orbit perturbation. The simulation shown in Figure 10 was generated using an effective Hamiltonian which includes the off-diagonal spin-orbit interaction derived from one-dimensional calculations, however the splitting is not readily visible on this scale [71]. Based on preliminary calculations of the bound states on the 3D spin-orbit corrected diabatic potential energy surfaces, it appears that the magnitude of the parity splittings for HCN-Br are smaller in a helium droplet than in the predicted gas-phase spectrum [52]. Interestingly this behavior would be opposite to that observed recently for NO, where an increase in the parity splitting was observed [72]. The spectroscopic constants derived from the fit to the HCN-Br spectrum are collected in Table VI. The rotational constant obtained from the simulation is 0.019 cm^{-1}, which can be compared with the zero-point corrected (B_0) values derived from the bound states on both the non-relativistic ($^2\Sigma$) and relativistic ($^2\Sigma_{1/2}$) 1D potential energy surfaces, namely 0.0623 and 0.0538 cm^{-1} respectively. As shown in the 1D potentials, and reflected in the B values, the spin-orbit coupling shifts the potential minimum to slightly longer internuclear distance. Since a fully quantitative theory for the reduction of rotational constants due to the helium is still lacking, we cannot definitively say which of these calculated B values is in better agreement with experiment, since both reduction factors are within the range typically observed. By comparing the B reductions for the HCN-Cl, HCN-Br, and HCN-I complexes however we do gain some insight into the accuracy of our relativistic potentials; see details below.

A Stark spectrum for HCN-Br is shown in Figure 10(C), recorded at an applied electric field strength of 2.25 kV cm^{-1}. The simulation includes the effects of the *e/f* symmetry splitting, however due to the mixing of J levels, its incorporation only slightly modifies the predicted spectrum. The peak marked with an asterix is ascribed to an impurity complex and likely contributes slightly to the congestion in the field-free spectrum. The ground and excited state dipole moments obtained from the simulation are 3.78 D, in excellent agreement with that found at the RMP2/aug-cc-pVTZ level (3.77 D).

HCN-I

Based on the pendular survey scans shown in Figure 6, we observe a pendular peak at 3309.37 cm^{-1} , which we tentatively assign a free stretch complex between HCN and an iodine atom. The field-free spectrum for this band is shown in Figure 11(A). Again the band shape is consistent with a molecule with no net orbital angular momentum (a Σ state), in agreement with the results for the HCN-Br complex. The observed frequency shift from HCN monomer is -1.83 cm^{-1}, which agrees nicely with the predicted increase in the binding energy upon vibrational excitation on the relativistic potentials, namely 1.63 cm^{-1}. The rotational constant derived from the simulation (B) is B = 0.016 cm^{-1} which is consistent with the results for HCN-Br. The corresponding value of the rotational constant derived from the lowest bound state of the $^2\Sigma_{1/2}$ potential is $B_0 = 0.04247$ cm^{-1}. Figure 11(C) also shows a Stark spectrum for HCN-I. The lines in the Stark spectrum appear to be much narrower than

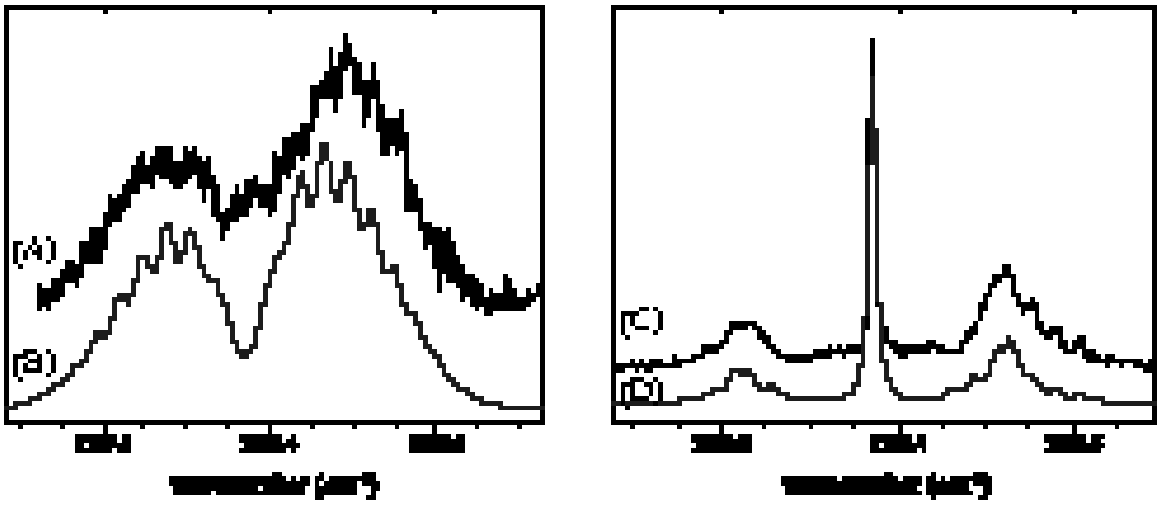

FIG. 11: The field-free (A) and Stark (C) infrared spectra of the CH stretching vibration of the HCN-I complex observed in helium droplets. The simulation of the field free spectrum (B) was used to determine the molecular constants and includes an off-diagonal spin-orbit perturbation, which however only slightly modifies the band shape at this resolution. Lorentzian linewidths of 0.025 and 0.01 cm^{-1} were used for fitting the field free and Stark spectra respectively.

in the corresponding field-free scan, which we attribute to considerable unresolved fine structure in field-free scan, which is decoupled by the field. Such fine structure is most likely caused by the spin-orbit coupling in this system, in analogy to that observed for HCN-Br. The electric field strength used to record the Stark spectrum (C) was not accurately calibrated and we can only say that the dipole moment is consistent with the *ab initio* value of 3.91 D.

THE HCN-Cl COMPLEX

When flowing Cl_2 through the hot pyrolysis source, no bands were observed that could be assigned to a hydrogen bound Cl-HCN complex. In the free stretch region however, a new peak is observed at 3309.33 cm^{-1} in good agreement with the previously observed bands for the HCN-Br (3309.55 cm^{-1}) and HCN-I (3309.37 cm^{-1}) complexes. The field-free and Stark spectra for HCN-Cl are shown in Figure 12(A) and (C) respectively. This new peak is only slightly shifted from the HCN-Cl_2 band, and thus the pyrolysis source was run at the highest possible temperatures to reduce the Cl_2 related signals. Unfortunately these conditions also lead to an increase in the amount of HCl produced in the source, presumably from the reaction of chlorine atoms with the quartz pyrolysis tube, and the HCN-HCl molecular complex is also observed. The assignment of this band to HCN-HCl was confirmed by a separate experiment in which HCl was intentionally introduced into the pick-up cell. Despite the overlap of two impurity complexes, we are able to reproduce all of the features of the spectrum, and extract the molecular parameters which are listed in Table VI. In the analysis of the spectrum we were not able to identify any fine structure that could be attributed to a spin-orbit interaction, which we tentatively assigned in the bromine and iodine complexes. This is consistent with the much smaller spin-orbit coupling constant for atomic chlorine compared to bromine or iodine. Indeed a simulation of the HCN-Cl spectra using the effective Hamiltonian developed for the HCN-Br, shows no such splittings at the experimental resolution.

The vibrational band origin of HCN-Cl is shifted from HCN monomer by -1.87 cm^{-1}. The *ab initio* frequency calculations predict a shift of -2.09 cm^{-1} at the RMP2/aug-cc-pVTZ level (see Table II) in good agreement with the experimental value. The shift predicted from the change in the binding energy upon vibrational excitation from 1D potential energy surfaces is -2.08 cm^{-1}. This value is nearly identical to the non-relativistic results due to the relatively small spin-orbit coupling constant for chlorine atoms. Bound state calculations predict that the isotope splitting between HCN-^{35}Cl and HCN-^{37}Cl is approximately 0.001 cm^{-1}, which is negligible at our resolution. In contrast, the two isotopes of Cl-HF were found to have a much larger splitting (0.038 cm^{-1}), due to the fact that it is a hydrogen bound complex [12, 68].

The rotational constant deduced from the fit to the spectrum is 0.032 cm^{-1}. Because the spin-orbit coupling is small in this case, the predicted rotational constants from the bound states on the $^2\Sigma$ and $^2\Sigma_{1/2}$ potentials are very similar, namely B_0= 0.08478 (0.08784) cm^{-1} for HCN-^{35}Cl on the $^2\Sigma_{1/2}$ ($^2\Sigma$) potential. The reduction of the rotational constant upon solvation is thus a factor of approximately 2.7. If we assume that the solvation behavior between the HCN-Cl, HCN-Br, and HCN-

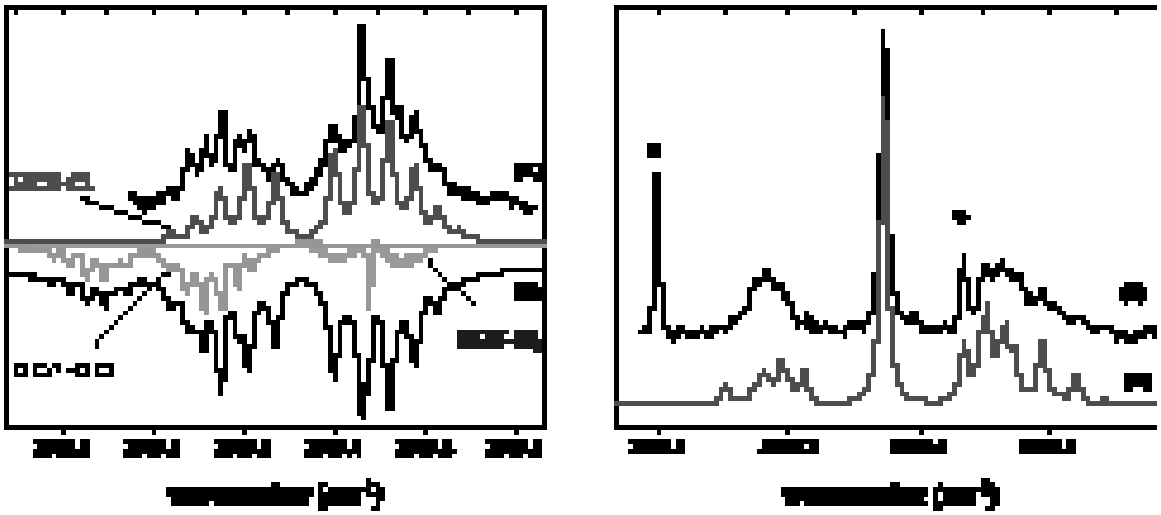

FIG. 12: (Left panel) (A) A rotationally resolved spectrum of the ν_{CH} band of the HCN-Cl complex in helium nanodroplets. The spectrum also has features due to both the HCN-HCl and HCN-Cl_2 complexes which overlap in this frequency region. Trace (B) is a summation of the 3 bands. (Right panel) (C) An experimental Stark spectrum of the corresponding band taken in the presence of a 2.833 kV cm^{-1} electric field. (D) A simulation of the experimental spectrum based only on the molecular parameters for HCN-Cl. The peaks marked with an asterix are due to the overlapping bands. Lorentzian linewidths of 0.028 and 0.013 cm^{-1} were used for fitting the field free and Stark HCN-Cl spectra respectively.

I complexes is the same, then this reduction factor also gives support to our earlier comparison of HCN-Br and HCN-I with the B values obtained from the spin-orbit corrected potentials. On these potentials the reduction factor was also determined to be 2.75, however if we had compared the experimental value to the B value from the non-relativistic potentials, the B reduction would have been 3.2.

Figure 12(C) also shows a Stark spectrum for HCN-Cl recorded at an applied field strength of 2.833 kV cm^{-1}. The dipole moment determined from the fit is 3.0(2) D, which is significantly smaller than the *ab initio* value of 3.66 D. It is interesting to note that the *ab initio* calculations are in better agreement for bromine than for chlorine what could be due to vibrational averaging over the low frequency bending and stretching modes of the complex. This would be more important for Cl due to its lighter mass, reducing the dipole moment from its equilibrium value. Indeed a similar trend was also observed for the X-HF complexes.

Constant	HCN-Cl	HCN-Br	HCN-I
ν (cm^{-1})	3309.33	3309.55	3309.37
B (cm^{-1})	0.032	0.019	0.016
D (cm^{-1})	5.0×10^{-5}	1.2×10^{-5}	1.0×10^{-5}
μ (D)	3.0	3.78	-

TABLE VI: The experimental spectroscopic constants obtained from a fit to the infrared spectra for each of the prereactive HCN-X complexes. Fine structure is observed in the HCN-Br and HCN-I spectra, which is attributed to spin-orbit interaction. A more detailed theoretical treatment for this effect is given elsewhere [71].

DI-RADICAL Br-HCCCN-Br COMPLEXES

Given the observation of the HCN-Br, Br-HCN, HCN-I, and I-HCN complexes, it is interesting to consider the possibility of picking up two halogen atoms, to form a di-radical complex such as Br-HCN-Br, which utilizes the HCN as a stabilizer, preventing the recombination to form HCN + Br_2. Such complexes would represent the beginnings of nano-scale radical solids which could be used as high-energy density materials [73]. Gordon *et al.* proposed a similar mechanism was responsible for the stabilization of nitrogen atoms in a N_2 matrix (of up to 10% atomic concentration) frozen in bulk liquid helium [74, 75, 76, 77, 78, 79]. While we have yet to perform extensive searches for HCN, we did explore this possibility for Br atoms and cyanoacetylene (HCCCN), where better signals are observed. Figure 13 shows a set of pendular survey scans covering the important frequency region. It is important to note that scans 13(A) - (C) were recorded by picking up the HCCCN first, but in 13(D) the order has been reversed, and we instead pickup from the pyrolysis source first. In Figure 13(A), only HCCCN is added to the droplets, while in 13(B), Br_2 is flowing through a room temperature pyrolysis source. The result of heating the pyrolysis to the appropriate temperatures for bromine atom pick-up are shown in Figures 13(C) and (D). In good agreement with the results of X + HCN, we find two peaks at 3326.1 and 3302.4 cm^{-1} (labeled by a

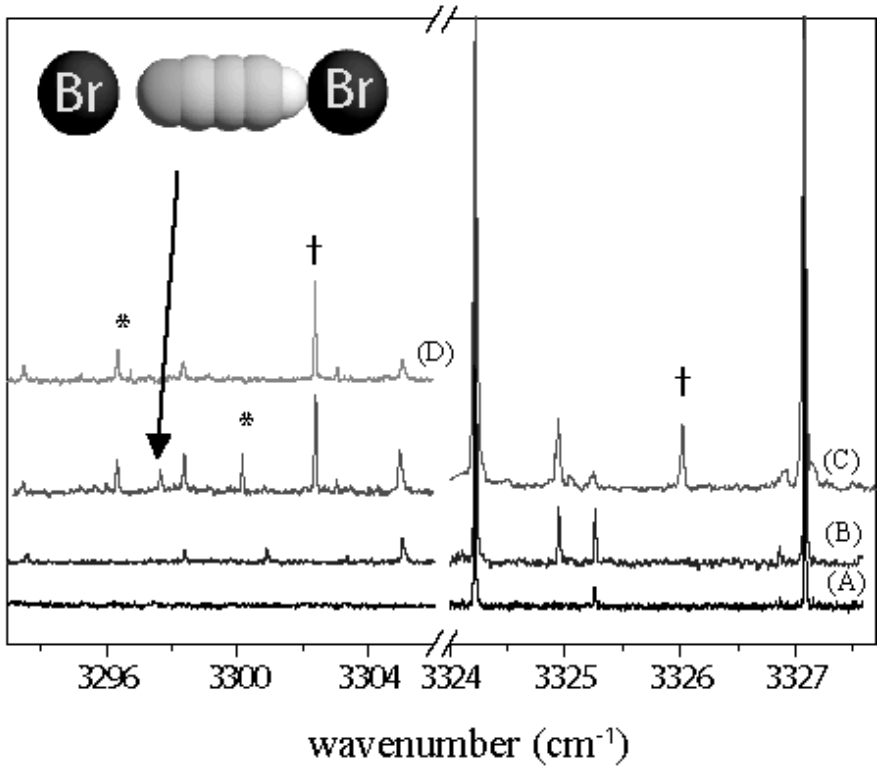

FIG. 13: A series of pendular scans for Br + HCCCN where the bromine pressure is intentionally high to facilitate forming larger clusters. In (A) only HCCCN is picked up by the droplets and in (B) Br_2 is flowing through the cold pyrolysis source. Scans (C) and (D) were recorded with the pyrolysis source at the appropriate temperature for bromine atom production, but for (D) the bromine is picked up first where as in (C) the cyanoacetylene is picked up first. The two peaks marked with a † are assigned to the linear Br-HCCCN and HCCCN-Br complexes, respectively. The two peaks marked with an * are found to optimize at higher HCCCN pressure and therefore correspond to more than one HCCCN. The peak at 3297.65 cm^{-1} optimizes at the same HCCCN pressure as the 1:1 complexes however is found to optimize at higher bromine pressure, suggesting that it is a complex containing two bromine radicals. The different behavior based on pick-up order is expected, since in (D) two bromine atoms will likely recombine to form Br_2 in the absence of the HCCCN.

† in the figure) which we assign to the Br-HCCCN and HCCCN-Br complexes, based on their frequency shifts and signal strengths. The peaks labeled with an * were found to optimize at higher HCCCN pressure, so they correspond to complexes containing more than one HCCCN. The peak at 3297.65 cm^{-1} is a good candidate for being Br-HCCCN-Br because it only appears in the spectrum when the HCCCN is picked up first. This dependence on pick-up order is to be expected because two bromine atoms will likely recombine to form Br_2 in the absence of the molecular spacer. To aid in this preliminary assignment we performed bromine pressure dependence measurements which are shown in Figure 14.

This new peak is found to optimize at higher bromine pressures than those peaks assigned to the 1:1 complexes, and agrees well with a simulation of a dimer using a Poisson distribution for the pick-up statistics. For these pick-up "cell" pressure dependence measurements the main chamber ion-gauge was used as the x-axis, however since this really monitors recombined Br_2 after collisions with the walls, instead of the local pressure of Br atoms in the pick-up zone, the pick-up curve for the dimer does not correspond to twice the optimum monomer pressure. Although we cannot rule out that a Br-HCCCN-Br_2, or similar complex might have such a pick-up cell pressure

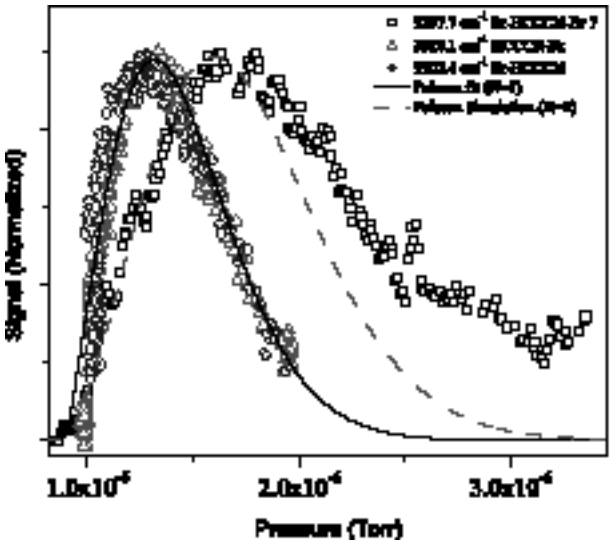

FIG. 14: Bromine pressure dependencies for the peaks assigned to the Br-HCCCN, HCCCN-Br, and Br-HCCCN-Br complexes. The fact that the peak at 3297.65 cm^{-1} optimizes at higher bromine pressure than the 1:1 complexes lends supporting evidence to our claim that this is a di-radical complex. The smooth curves are the calculated pick-up probabilities obtained by fitting a Poisson distribution to the 1:1 curve, and then re-simulating the curve for the dimer.

dependence, a double-resonance population transfer experiment [80] in which this new peak is pumped and the HCCCN-Br_2 complex is recovered would be definitive.

DISCUSSION

Extensive pendular survey scans have been performed in order to find evidence for the entrance channel complexes of fluorine atoms with HCN. From the *ab initio* calculations presented above, it is clear that the reaction to form the HFCN product is quite exothermic, and exhibits only a small barrier, if any, to the reaction. The calculated energies of the HFCN product and its barrier relative to F + HCN are -34.05 and -2.45 kcal mol^{-1} (-28.44 and 3.05 kcal mol^{-1}), respectively, at the G2 (UCCSD(T)/6-311++G(d,p)) level of theory. Two entrance channel complexes (F-HCN and HCN-F) were also found in the G2 calculations with energies -0.55 and -1.58 kcal mol^{-1} respectively. The unintuitive result that the transition state is calculated (at the G2 level) to be lower in energy than the corresponding van der Waals minima is simply an artifact of the calculation, and this small energy difference is within the estimated accuracy of the method. The fact that we do not observe a fluorine atom pre-reactive complex could be an indication that indeed the insertion reaction takes place, even under our experimental conditions at 0.37 K. This conclusion is also partially supported by the argon matrix work of Andrews [38] and Misochko [39] where the insertion product has been identified. No pre-reactive complexes were observed in these works. Guided by their observed frequency of the CH stretching vibration of 3018 cm^{-1}, we searched for HFCN in helium. No signals were observed, however this frequency range is at the edge of the tuning range of the lasers used in this work. The oscillator strength for this vibration is also approximately 50 times weaker than the HCN fundamental, based on harmonic frequency calculations, and thus the argon matrix experiment has the big advantage of concentrating the product using longer deposition times. We hope to revisit this experiment using newer technology OPO lasers, with a larger tuning range and higher output power [81, 82].

Due to the statistical nature of the pick-up process it should be possible to "tag" the HFCN product with another weakly bound molecule, which could then act as a stronger infrared chromophore. Indeed we have preliminary evidence that such a situation also arises in reaction of aluminum atoms with HCN and HF [83]. Shown in Figure 15 is a two-dimensional angular potential for HCN + HFCN calculated at the RMP2/aug-cc-pVDZ level, which shows that multiple van der Waals isomers may indeed exist. Since cluster formation in helium occurs sequentially and obeys Poisson statistics, these clusters should be formed when picking up HCN after the fluorine atom, given that the droplet is large enough to stabilize the HFCN. Based on the calculated exothermicity, the formation of HFCN would boil off approximately 2500 helium atoms (assuming 5 cm^{-1} per atom [44]).

The last remaining question in this study is the existence of a hydrogen bound Cl-HCN complex in analogy with that observed for bromine and iodine atoms. Due to the fact that the isomerization barriers between the hydrogen and nitrogen bound isomers are so small, one possible explanation is that this isomer is not formed due to a zero-point energy effect, and that the complex simply converts to the global minimum HCN-Cl isomer. To make any further analysis of this possibility we must await the spin-orbit corrected 2D potentials [52], to get a more realistic view of how the isomerization barrier is effected by spin-orbit coupling. A second possibility is that the reactivity is enhanced when the chlorine atom approaches the hydrogen end of HCN and it reacts, in analogy with that proposed for F + HCN.

SUMMARY

We have presented here a combined experimental and theoretical investigation of the halogen atom - HCN entrance channel complexes in order to compare with the X-HF complexes studied previously. The potential energy surfaces for X + HCN are found to be considerably more complex than for X+HX, due to the possibility of hydrogen atom abstraction and addition reactions. The

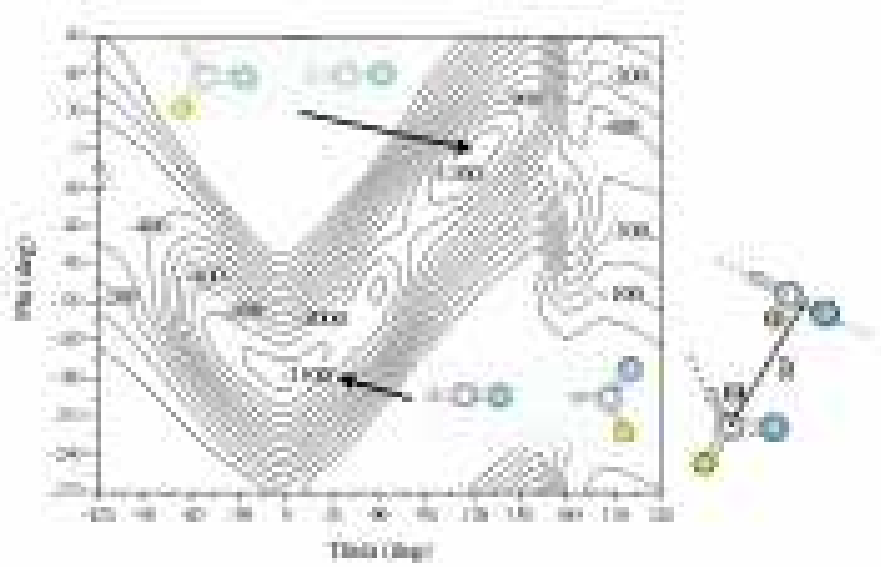

FIG. 15: A two-dimensional interaction potential calculated at the RMP2/aug-cc-pVDZ level for the insertion product HFCN with a second HCN molecule. The second HCN molecule was assumed to lie in the plane of HFCN due to the fact that no non-planar geometries were observed in fully relaxed optimizations. The two angles were stepped in increments of 15° and only the intermolecular distance was allowed to optimize in the calculation. Counterpoise correction was applied and a spline interpolation used to generate the final surface. Contour lines are drawn in 100 cm^{-1} intervals. By tagging the F + HCN reaction product with a second HCN molecule, we regain a strong high-frequency CH stretch which could be then probed experimentally.

lone pair on the nitrogen of HCN is also found to significantly alter the shape of the long-range potential energy surfaces, and for X + HCN, we find that the global minimum is a linear nitrogen bound geometry in contrast to the hydrogen bound global minimum for X-HF. A linear hydrogen bound X-HCN complex is also predicted to be stable, however the isomerization barrier back to the global minimum is small. *Ab initio* calculations predict that for iodine and bromine significant barriers to the chemical reactions exist, and thus the entrance channel complexes should be quite stable when formed in a helium droplet. Both of the linear van der Waals isomers predicted by theory are observed experimentally for bromine and iodine atoms. Interestingly a HCN-Cl isomer was also observed whereas Cl-HCN was not. Since HCN-Cl is predicted to be the global minimum on the van der Waals potential, it could be that the isomerization barrier is simply too small to prevent Cl-HCN from rearranging to HCN-Cl. A second possibility is that the reactivity is enhanced on the hydrogen end of HCN, and Cl-HCN goes on to react to form HClCN. No entrance channel complexes were observed in the fluorine experiments, and we preliminarily interpret this as a result of reaction. The intermediate reaction product HFCN has been recently observed in an argon matrix, however, also in that work no pre-reactive complexes were observed. Preliminary searches for HFCN in this work in helium nanodroplets did not reveal this species. The photon energy used to study the CH stretching vibration of the entrance channel complexes is greater than the predicted barriers, suggesting that photo-initiation of the corresponding reactions could be possible. The unique asymptotic degeneracy of the multiple electronic states in the region of the entrance and exit channels for free radical - molecule complexes is found to give rise to fine structure in the observed spectra for HCN-Br and HCN-I.

ACKNOWLEDGMENTS

The authors wish to thank Anna Fishchuk and Ad van der Avoird for their theoretical work on these X-HCN systems and its correspondence before publication. This work was supported by the Air Force Office of Scientific Research (AFOSR). Partial support is also acknowledged

from the National Science Foundation (CHE-99-87740). J. K. acknowledges financial support of the Alexander von Humboldt foundation through a Feodor Lynen fellowship.

* Electronic address: merritjm@unc.edu
§ Present address: Fritz-Haber-Institut der MPG, Faradayweg 4-6, 14195 Berlin, Germany
† Deceased: Nov 6, 2005

[1] J. M. Hutson, *Annu. Rev. Phys. Chem.*, 1990, **41**, 123–154.
[2] M. I. Lester, B. V. Pond, M. D. Marshall, D. T. Anderson, L. B. Harding, and A. F. Wagner, *Faraday Disc.*, 2001, **118**, 373–385.
[3] Y. L. Chen and M. C. Heaven, *J. Chem. Phys.*, 1998, **109**(13), 5171–5174.
[4] M. C. Heaven, *Int. Rev. Phys. Chem.*, 2005, **24**, 375–420.
[5] T. C. McInnis and L. Andrews, *J. Phys. Chem.*, 1992, **96**(5), 2051–2059.
[6] E. Y. Misochko, V. A. Benderskii, A. U. Goldschleger, A. V. Akimov, and A. F. Shestakov, *J. Am. Chem. Soc.*, 1995, **117**, 11997–11998.
[7] R. D. Hunt and L. Andrews, *J. Chem. Phys.*, 1988, **88**, 3599–3606.
[8] K. Nauta and R. E. Miller, *Science*, 1999, **283**, 1895–1897.
[9] K. Nauta and R. E. Miller, *Science*, 2000, **287**, 293–295.
[10] F. Madeja, M. Havenith, K. Nauta, and R. E. Miller, *J. Chem. Phys.*, 2004, **120**, 10554.
[11] F. Stienkemeier, W. E. Ernst, J. Higgins, and G. Scoles, *J. Chem. Phys.*, 1995, **102**, 615–617.
[12] J. M. Merritt, J. Küpper, and R. E. Miller, *Phys. Chem. Chem. Phys.*, 2005, **7**(1), 67–78.
[13] J. M. Merritt, S. Rudić, and R. E. Miller, *J. Chem. Phys.*, 2006, **124**, 084301–084313.
[14] S. Rudić, J. M. Merritt, and R. E. Miller, *J. Chem. Phys.*, 2006, **124**, 104305.
[15] N. Balakrishnan, *J. Chem. Phys.*, 2004, **121**(12), 5563–5566.
[16] D. Skouteris, D. E. Manolopoulos, W. Bian, H. J. Werner, L. H. Lai, and K. Liu, *Science*, 1999, **286**, 1713–1716.
[17] P. F. Weck and N. Balakrishnan, *Int. Rev. Phys. Chem.*, 2006, **25**, 283.
[18] D. Towsend, S. A. Lahankar, S. K. Lee, S. D. Chambreau, A. G. Suits, X. Zhang, J. Rheinecker, L. B. Harding, and J. M. Bowman, *Science*, 2005, **306**, 1158.
[19] X. Zhang, J. Rheinecker, and J. M. Bowman, *J. Chem. Phys.*, 2005, **122**, 114313.
[20] C. S. Maierle, G. C. Schatz, M. S. Gordon, P. Mccabe, and J. N. Connor, *J. Chem. Soc. Faraday Trans.*, 1997, **93**, 709–720.
[21] W. B. Zeimen, J. Klos, G. C. Groenenboom, and A. van der Avoird, *J. Phys. Chem. A*, 2003, **107**, 5110–5121.
[22] G. W. M. Vissers and A. B. McCoy, *J. Phys. Chem. A*, 2006, **110**, 5978–5981.
[23] W. B. Zeimen, J. Klos, G. C. Groenenboom, and A. van der Avoird, *J. Phys. Chem. A*, 2004, **107**, 9319–9322.
[24] M. P. Deskevich, M. Y. Hayes, K. Takahashi, R. T. Skodje, and D. J. Nesbitt, *J. Chem. Phys.*, 2006, **124**, 224303.
[25] P. Zdanska, D. Nachtigallova, P. Nachtigall, and P. Jungwirth, *J. Chem. Phys.*, 2001, **115**(13), 5974–5983.
[26] M. Meuwly and J. M. Hutson, *J. Chem. Phys.*, 2000, **112**(2), 592–600.
[27] J. Klos, M. M. Szczesniak, and G. Chalasinski, *Int. Rev. Phys. Chem.*, 2004, **23**, 541–571.
[28] C. Kreher, R. Theinl, and K. H. Gericke, *J. Chem. Phys.*, 1996, **104**(12), 4481.
[29] B. K. Decker, G. He, I. Tokue, and R. G. Macdonald, *J. Phys. Chem. A*, 2001, **105**(24), 5759–5767.
[30] R. B. Metz, J. M. Pfeiffer, J. D. Thoemke, and F. F. Crim, *Chem. Phys. Lett.*, 1994, **221**, 347–352.
[31] D. Troya, M. Gonzalez, G. S. Wu, and G. C. Schatz, *J. Phys. Chem. A*, 2001, **105**(11), 2285–2297.
[32] L. B. Harding, *J. Phys. Chem.*, 1996, **100**, 10123–10130.
[33] J. de Juan, S. Callister, H. Reisler, G. A. Segal, and C. Wittig, *J. Chem. Phys.*, 1988, **89**, 1977–1985.
[34] I. R. Sims and I. W. M. Smith, *J. Chem. Soc. Faraday Trans. 2*, 1989, **85**, 915–923.
[35] M. J. Frost, I. W. M. Smith, and R. D. Spencer-Smith, *J. Chem. Soc. Faraday Trans. 2*, 1993, **89**, 2355.
[36] J. M. Pfeiffer, R. B. Metz, J. D. Thoemke, E. Woods, and F. F. Crim, *J. Chem. Phys.*, 1995, **104**, 4490–4501.
[37] C. Kreher, J. L. Rinnenthal, and K. H. Gericke, *J. Chem. Phys.*, 1998, **108**, 3154–3167.
[38] R. D. Hunt and L. Andrews, *Inorg. Chem.*, 1987, **26**, 3051–3054.
[39] I. U. Goldschleger, A. V. Akimov, E. Y. Misochko, and C. A. Wight, *Mendeleev Comm.*, 2001, (2), 43–45.
[40] K. Nauta and R. E. Miller, *J. Chem. Phys.*, 1999, **111**, 3426–3433.
[41] E. L. Knuth, B. Schilling, and J. P. Toennies, Oxford University Press, Oxford, 1995; Vol. 19, pp. 270–276.
[42] J. Küpper, J. M. Merritt, and R. E. Miller, *J. Chem. Phys.*, 2002, **117**(2), 647–652.
[43] K. Nauta and R. E. Miller, *J. Chem. Phys.*, 2001, **115**(22), 10138–10145.
[44] D. M. Brink and S. Stringari, *Z. Phys. D*, 1990, **15**, 257–263.
[45] G. E. Douberly and R. E. Miller, *J. Phys. Chem. B*, 2003, **107**(19), 4500–4507.
[46] S. F. Boys and F. Bernardi, *Mol. Phys.*, 1970, **19(4)**, 553–566.
[47] A. C. Legon and J. C. Thorn, *J. Chem. Soc. Faraday Trans.*, 1993, **89**(23), 4157–4162.
[48] K. Hinds and A. C. Legon, *Chem. Phys. Lett.*, 1995, **240**, 467–473.
[49] A. C. Legon and K. Hinds, *Mol. Phys.*, 1996, **88**(3), 673–682.
[50] L. A. Curtiss, K. Raghavachari, G. W. Trucks, and J. A. Pople, *J. Chem. Phys.*, 1991, **94**(11), 7221.
[51] M. W. Chase Jr, *J. Phys. Chem. Ref. Data*, 1998, **4**(9), 1–1951.
[52] A. Fishchuk, J. M. Merritt, and A. van der Avoird, in preparation, 2006.
[53] H. J. Werner, P. J. Knowles, R. D. Amos, A. Bernhardsson, A. Berning, P. Celani, D. L. Cooper, M. J. O. Deegan, A. J. Dobbyn, F. Eckert, C. Hampel, G. Hetzer, T. Korona, R. Lindh, A. W. Lloyd, S. J. McNicholas, F. R. Manby, W. Meyer, M. E. Mura, A. Nicklass, P. Palmieri, R. Pitzer, G. Rauhut, M. Schutz,

U. Schumann, H. Stoll, A. J. Stone, R. Tarroni, and T. Thorsteinsson, *MOLPRO, A package of Ab initio Programs, version 2002.1*, University College Cardiff Consultants Limited, Wales, UK, 2002.

[54] J. Klos, G. Chalasinski, H. Werner, and M. M. Szczesniak, *J. Chem. Phys.*, 2003, **115**(7), 3085–3098.

[55] F. M. Tao and Y. K. Pan, *J. Chem. Phys.*, 1992, **97**(7), 4989–4995.

[56] A. V. Fishchuk, P. E. S. Wormer, and A. van der Avoird, *J. Phys. Chem. A*, 2006, **110**(16), 5273–5279.

[57] K. A. Peterson, D. Figgen, E. Goll, H. Stoll, and M. Dolg, *J. Chem. Phys.*, 2003, **119**(21), 11113–11123.

[58] M. Meuwly and J. M. Hutson, *Phys. Chem. Chem. Phys.*, 2000, **2**(4), 441–446.

[59] H. Lefebvre-Brion and R. W. Field, *Perturbations in the Spectra of Diatomic Molecules*, Academic Press, Orlando, Fl., 1986.

[60] J. E. Rode, J. Klos, L. Rajchel, M. Szczeniak, G. Chalasinski, and A. A. Buchachenko, *J. Phys. Chem. A*, 2005, **109**, 11484–11494.

[61] A. Nicklass, K. A. Peterson, A. Berning, H. J. Werner, and P. J. Knowles, *J. Chem. Phys.*, 2000, **112**(13), 5624–5632.

[62] R. J. LeRoy, Level 7.7: A computer program for solving the radial schrödinger equation for bound and quasibound levels University of Waterloo Chemical Physics Research Report CP-661; see the "computer programs" link at http://leroy.uwaterloo.ca, 2005.

[63] K. Nauta, D. T. Moore, and R. E. Miller, *Faraday Disc.*, 1999, **113**, 261–278.

[64] E. W. Draeger and D. M. Ceperley, *Phys. Rev. Lett.*, 2003, **90**(6), 065301.

[65] R. A. Frosh and H. M. Foley, *Phys. Rev.*, 1952, **88**(6), 1337–1349.

[66] J. Brown and A. Carrington, *Rotational Spectroscopy of Diatomic Molecules*, Cambridge molecular science, 2003.

[67] M. Y. Choi, G. E. Douberly, T. M. Falconer, W. K. Lewis, C. M. Lindsay, J. M. Merritt, P. L. Stiles, and R. E. Miller, *Int. Rev. Phys. Chem.*, 2006.

[68] A. V. Fishchuk, G. C. Groenenboom, and A. van der Avoird, *J. Phys. Chem. A*, 2006, **110**(16), 5280–5288.

[69] V. Jaccarino, J. G. King, R. A. Satten, and H. H. Stroke, *Phys. Rev.*, 1954, **94**, 1798–1799.

[70] H. H. Brown and J. G. King, *Phys. Rev.*, 1966, **142**(1), 53–59.

[71] J. M. Merritt and R. W. Field, in preparation, 2006.

[72] K. von Haeften, A. Metzelthin, S. Rudolph, V. Staemmler, and M. Havenith, *Phys. Rev. Lett.*, 2005, **95**(21), 215301.

[73] F. Cacace, G. de Petris, and A. Troiani, *Science*, 2002, **295**, 480–481.

[74] E. B. Gordon, V. V. Khmelenko, A. A. Pelmenev, E. A. Popov, and O. F. Pugachev, *Chem. Phys. Lett.*, 1989, **155**, 301–304.

[75] R. E. Boltnev, E. B. Gordon, V. V. Khmelenko, I. N. Krushinskaya, M. V. Martynenko, A. A. Pelmenev, E. A. Popov, and A. F. Shestakov, *Chem. Phys.*, 1994, **189**, 367–382.

[76] E. B. Gordon, A. A. Pelmenev, O. F. Pugachev, and V. V. Khmelenko, *Chem. Phys.*, 1981, **61**, 35–41.

[77] E. B. Gordon, L. P. Mezhov-Deglin, O. F. Pugachev, and V. V. Khmelenko, *Chem. Phys. Lett.*, 1978, **54**(2), 282–285.

[78] E. B. Gordon, V. V. Khmelenko, A. A. Pelmenev, E. A. Popov, O. F. Pugachev, and A. F. Shestakov, *Chem. Phys.*, 1993, **170**, 411–426.

[79] R. E. Boltnev, E. B. Gordon, I. N. Krushinskaya, M. V. Martynenko, A. A. Pelmenev, E. A. Popov, V. V. Khmelenko, and A. F. Shestakov, *Low Temp. Phys.*, 1997, **23**, 567–577.

[80] G. E. Douberly, J. M. Merritt, and R. E. Miller, *Phys. Chem. Chem. Phys.*, 2005, **7**(3), 463–468.

[81] J. M. Merritt, *Ph.D. Dissertation, University of North Carolina at Chapel Hill*, 2006.

[82] F. J. M. Harren, S. Li, S. E. Bisson, and M. M. J. W. V. Herpen, *Appl. Phys. B*, 2002, **75**, 329–333.

[83] J. M. Merritt, G. E. Douberly, P. L. Stiles, and R. E. Miller, in preparation, 2006.

[84] The P(4) transition of the (004) ← (000) band (12623 cm^{-1}) and the P(8) transition of the (302) ← (000) band (12631 cm^{-1}) were used for the excitation